Journal of Organometallic Chemistry, 367 (1989) 275–289
Elsevier Sequoia S.A., Lausanne – Printed in The Netherlands
JOM 09758

The syntheses, structures, and stereodynamics of [3]ferrocenophane complexes

I. Group 6 metal tetracarbonyl complexes, *cis*-$[M(CO)_4\{(C_5H_4ECH_3)_2Fe\}]$. (M = Cr, Mo, W; E = S or Se). Crystal structure of 1,1′-bis(methylseleno)ferrocene tetracarbonyltungsten

Edward W. Abel, Nicholas J. Long, Keith G. Orrell, Anthony G. Osborne, Vladimir Šik

Department of Chemistry, The University, Exeter, Devon EX4 4QD (Great Britain)

Paul A. Bates and Michael B. Hursthouse

Department of Chemistry, Queen Mary College, London E1 4NS (Great Britain)

(Received December 5th, 1988)

Abstract

The complexes *cis*-$[M(CO)_4\{(C_5H_4ECH_3)_2Fe\}]$ (M = Cr, Mo or W; E = S or Se) have been synthesised. Pyramidal inversion of the coordinated S or Se atoms was arrested in most cases at low temperatures ($\sim -80\,^\circ$C), when the DL forms of the complexes predominated ($\geq 78\%$). At higher temperatures combined 1D and 2D-EXSY NMR studies led to energies ($\Delta G^\ddagger$(298 K) values) for chalcogen inversion in the range 31–50 kJ mol^{-1}. Fairly large $\Delta S^\ddagger$ values for these processes were attributed to the rapid reversal of the $EM(CO)_4E$ portion of the ferrocenophane ring. The crystal structure of 1,1′-bis(methylseleno)ferrocene tetracarbonyltungsten has been determined. The crystals have space group $P2_1/a$ with a 17.580(3), b 9.665(1), c 11.059(1) Å, β 107.33(1)° and $Z = 4$. Least-squares refinement gave $R = 0.031$ for 2369 independent significant reflections. The W–Se bond lengths are 2.674(4) and 2.692(4) Å, and the Se–Me groups adopt a DL relationship. The Se–W–Se bond angle is 86.3° and the non-bonded Se–Se separation 3.67 Å. The cyclopentadienyl rings adopt an eclipsed conformation with the ring planes parallel.

0022-328X/89/$03.50

Introduction

The stereodynamics of chalcogen atoms when part of a ligand coordinated to a transition metal are readily studied by NMR spectroscopy. In recent years a considerable variety of complexes has been investigated by variable temperature NMR which has enabled a number of novel intramolecular rearrangements to be identified, and their energy barriers determined [1,2]. The most common of these motions is the pyramidal inversion of the chalcogen atom.

As part of a continuing study of the various factors affecting chalcogen inversion energies in transition metal complexes of chalcogen-containing ligands we have initiated a study of complexes of the ligands 1,1′-bis(methylthio)ferrocene (BMSF) and 1,1′-bis(methylseleno)ferrocene (BMSEF). The formation of chelate complexes with these ligands converts the ferrocenyl moiety into a [3]ferrocenophane and hence the occurrence of both ferrocenophane bridge reversal and pyramidal chalcogen inversion can be expected. Also the low torsional barriers between the cyclopentadienyl rings endow the system with a high degree of flexibility and hence contrasts with the more rigid ligands with a hydrocarbon backbone which have been previously studied. In this paper we report the synthesis and spectroscopic properties of the complexes $[M(CO)_4(BMSF)]$ and $[M(CO)_4(BMSEF)]$ (M = Cr, Mo, W), the chalcogen inversion energies of $[M(CO)_4(BMSF)]$ (M = Cr), and $[M(CO)_4$-(BMSEF)] (M = Cr, Mo, W), and the crystal and molecular structure of $[W(CO)_4$-(BMSEF)].

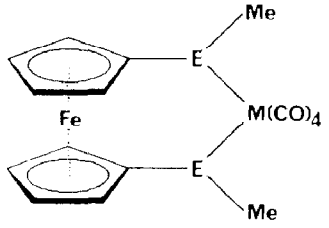

1	E = S	M = Cr
2	E = Se	M = Cr
3	E = S	M = Mo
4	E = Se	M = Mo
5	E = S	M = W
6	E = Se	M = W

Experimental

General

All preparations were carried out using standard Schlenk techniques [3]. The solvents were freshly distilled, dried and degassed before use and all reactions were performed under purified nitrogen.

The following complexes were prepared according to literature methods; *cis*-$[M(CO)_4(nbd)]$ (M = Cr, Mo) [4], (nbd = bicyclo[2.2.1]-hepta-2,5-diene), (M = W) [5], *fac*-$[M(CO)_3(NCCH_3)_3]$ (M = W) [6].

Infrared spectra were recorded on a Perkin–Elmer 881 infrared spectrophotometer, calibrated from the 1602 cm^{-1} signal of polystyrene.

Elemental analyses were performed by Butterworth Laboratories Ltd., Teddington, Middlesex, London and by C.H.N. Analysis, South Wigston, Leicester.

Synthesis of ligands.

1,1′-Bis(methylthio)ferrocene (BMSF). This ligand was prepared according to the method described by McCulloch et al. [7].

1,1′-Bis(methylseleno)ferrocene (BMSEF). This ligand was prepared in an analogous fashion to BMSF, except that methyldiselenide was used and, for purification, the product was subjected to dry-column chromatography on neutral grade II alumina. Elution with hexane produced a broad, orange band, which after collection and removal of the solvent under reduced pressure, left the ligand as a foul-smelling, dark orange, viscous oil. Yield 2.44 g (41%). ^{1}H NMR data ($CDCl_3$ solution): δ 2.15(t), CH_3Se (^2J(HSe) = 11.3 Hz); 4.20(t), *H*(3,4) (ring protons); 4.31(t), *H*(2,5) (ring protons).

Synthesis of complexes

All the complexes were prepared in a similar way, the only difference being the time of reaction. A representative example is outlined below, with details of all the synthetic, analytical and infrared data summarised in Table 1.

$[Mo(CO)_4(nbd)]$ (0.30 g, 1.0 mmol) was dissolved in hexane (40 cm^3), BMSF (0.278 g, 1.0 mmol) was added and the solution stirred. The mixture was refluxed for 20 h and a small amount of a fine, pale orange precipitate formed with an orange, supernatant liquid. The suspension was filtered and the filtrate evaporated to dryness, then sparingly washed with cold hexane. Both of the solid extracts were separately recrystallised from dichloromethane/hexane (1/2) to produce orange crystals of *cis*-$[Mo(CO)_4(BMSF)]$. Total yield, 0.135 g (28%).

NMR studies

^{1}H, ^{13}C-{^{1}H} and ^{77}Se-{^{1}H} NMR spectra were recorded on a Bruker AM250 FT spectrometer, operating at 250.13, 62.90 and 47.70 MHz respectively. A ^{1}H 2D-NOESY spectrum of complex **5** was recorded on a 400 MHz spectrometer at the University of Warwick.

All spectra were recorded in $CDCl_3$ or CD_2Cl_2 solutions using Me_4Si as internal standard, except for the ^{77}Se NMR where Me_2Se_2 was used as external standard.

A standard B-VT1000 variable temperature unit was used to control the probe temperature, the calibration of this unit being checked periodically against a Comark digital thermometer. The temperatures are considered accurate to ± 1°C.

^{1}H 2D-EXSY spectra for complexes **2**, **4** and **6** were recorded as previously reported [8,9] using the Bruker automation program NOESYPH. In the two-dimensional experiments, the F1 dimension contained 64 words which was then zero-filled to 256 words, and the F2 dimension contained 256 words. The spectral width was 300 Hz. The mixing time, τ_m, was 1 s, with a maximum random variation of 10%. The number of scans per experiment was 32, giving a total experimental time of 2 h. The data were processed using a gaussian window function of size 1 Hz in both dimensions and symmetrised about the diagonal.

Bandshape analyses were performed using modified versions of the program DNMR of Kleier and Binsch [10,11].

X-ray structure determination

Crystal data for $C_{16}H_{14}FeO_4Se_2W$: M = 667.90, monoclinic, space group $P2_1/a$, a = 17.580(3), b = 9.665(1), c = 11.059(1) Å, β = 107.33(1)°, U = 1793.7(4) Å^3, Z = 4, D_c = 2.473 g cm^{-3}, F(000) = 1240, λ = 0.71069 Å, μ(Mo-K_α) = 113.92 cm^{-1}, crystal size 0.50 × 0.20 × 0.18 mm.

Data collection: Unit cell parameters and intensity data were obtained by

Table 1

Syntheses and characterisation of the complexes *cis*-[$M(CO)_4(L–L)$] (M = Cr, Mo, W: (L–L) = chelating ferrocenylchalcogenide)

Complex	Reaction time (h)	Yield [a] (%)	Melting point (°C)	ν(CO) [b] (cm^{-1})	Analytical data Found (calc) (%)	
					C	H
cis-[$Cr(CO)_4$(BMSF)] (1)	40	23	110–115(dec.)	2017m, 1905vs,br, 1858s	43.4 (43.4)	3.3 (3.2)
cis-[$Cr(CO)_4$(BMSEF)] (2)	40	33	125–130(dec.)	2014m, 1903vs,br, 1857s	36.0 (35.8)	2.7 (2.6)
cis-[$Mo(CO)_4$(BMSF)] (3)	20	28	148–150	2027m, 1914vs,br, 1859s	39.3 (39.5)	2.9 (2.9)
cis-[$Mo(CO)_4$(BMSEF)] (4)	32	34	129–131	2024m, 1913vs,br, 1859m	33.4 (33.1)	2.6 (2.4)
cis-[$W(CO)_4$(BMSF)] (5)	30	42	167–169	2021m, 1902vs,br, 1855s	33.4 (33.5)	2.5 (2.4)
cis-[$W(CO)_4$(BMSEF)] (6)	48	48	159–160	2019m, 1901vs,br, 1855s	28.9 (28.7)	2.2 (2.1)

[a] Yields quoted relative to *cis*-[$M(CO)_4$(nbd)]. [b] Recorded in CH_2Cl_2 solution.

following previously detailed procedures [12], using a CAD4 diffractometer operating in the ω-2θ scan mode, with graphite-monochromated Mo-K_α radiation.

A total of 3154 unique reflections were collected ($3 \leqslant 2\theta \leqslant 50°$). The segment of reciprocal space scanned was: h, 0–20; k, 0–11; l, −13–13. The reflection intensities were corrected for absorption, using the azimuthal-scan method [13]; maximum and minimum transmission factors 1.00, 0.67.

Solution and refinement of structure: The structure was solved by the application of routine heavy-atom methods (SHELX-84) [14], and refined by full-matrix least-squares (SHELX-76) [15]. All non-hydrogen atoms were refined anisotropically and hydrogen atoms were not included in the final model.

The final residuals R and R_w were 0.031 and 0.035 respectively for the 217 variables and 2369 reflections for which $F_o > 6\sigma(F_o)$. The function minimised was $\Sigma w(|F_o| - |F_c|)^2$, with the weight, w, being defined as $1/[\sigma^2(F_o) + gF_o^2]$, [$g$ = 0.003].

Atomic scattering factors and anomalous scattering parameters were taken from references [16] and [17] respectively *. All computations were made on a DEC VAX-11/750 computer.

Results and Discussion

NMR spectroscopy

All six complexes **1–6** were examined by variable temperature ^{1}H spectroscopy, and chemical shift values for ambient and low temperatures are collected in Table 2. Low temperature data are not quoted for the S ligand complexes *cis*-[$Cr(CO)_4$(BMSF)] and *cis*-[$Mo(CO)_4$(BMSF)] as their static spectra could not be obtained even at ca. −80 °C, at which temperature the complexes tended to precipitate from solution. The limiting low temperature spectra of the other complexes indicate the presence of two solution species of grossly unequal populations. In the ring proton region (δ 4.2–4.8) four intense multiplets due to a weakly coupled ABCD spin system were observed for all the complexes. Interspersed between these signals was a weaker set, three out of four normally being detected. On raising the temperature of the NMR sample, exchange broadening occurs between certain bands in the stronger and weaker sets of lines, until at room temperature two averaged signals were observed, consistent with an AA′BB′ spin system, although multiplet splittings were not revealed due to residual line broadening from the rate process involved.

Two possible intramolecular rate processes may be the cause of these dynamic NMR features, namely pyramidal inversion of the coordinated chalcogen atoms, and reversal of the $EM(CO)_4E$ portion of the ferrocenophane ring. If either or both processes are slow on the NMR timescale then four configurational isomers can exist, namely *meso*-1, *meso*-2 and a degenerate DL pair. These species may be related by the eight corners of a cube (Fig. 1), where chalcogen inversion will interconvert the four forms on the front and rear faces of the cube, and bridge

* A Table of observed and calculated structure amplitudes and a complete list of anisotropic thermal parameters have been deposited with the British Library at Boston Spa, Wetherby, LS23 7BQ (Great Britain) as Supplementary Publication No. SUP 90196.

Table 2

^{1}H NMR parameters for the complexes **1–6** in CD_2Cl_2 solution at ambient and low temperatures

Complex	Temperature (°C)	Solution species	Invertomer population (%)	δ(E–Me)	δ(ring)
1	30	[a]	100	2.59(s)	4.62(t) 4.32(t)
2	−30	DL	84	2.40(s)	4.49 [b] 4.38 4.35 4.26
		meso	16		4.80 [c] 4.19
	20	[a]	100	2.47(t)[9.2] [d]	4.51(t) 4.33(t)
3	20	[a]	100	2.27(s)	4.24(t) 4.18(t)
4	−60	DL	93	2.39(s)	4.46(m) 4.39(m) 4.29(m) 4.23(m)
		meso	7	2.47(s)	4.67(m) [c]
	30	[a]	100	2.50(t)[9.1] [d]	4.47(t) 4.36(t)
5	−90	DL	78	2.73(s)	4.49 [b] 4.44 4.37 4.24
		meso	22		4.77 [c] 4.53 4.19
	30	[a]	100	2.83(t)[2.5] [e]	4.60(t) 4.38(t)
6	−70	DL	90	2.56(s)	4.48(m) 4.40(m) 4.30(m) 4.24(m)
		meso	10	2.62(s)	4.69(m) [c] 4.44(m) 4.19(m)
	30	[a]	100	2.67(2×t)[9.1] [d] [2.4] [e]	4.50(t) 4.37(t)

[a] Averaged *meso*/DL species. [b] Signals not resolvable. [c] Some *meso* signals not observed due to overlap. [d] ^2J(SeH). [e] ^3J(WH).

reversal will exchange adjacent species on the front and rear faces. In such a representation diametrically opposite corners of the cube contain mirror image pairs of DL species and topomeric forms of *meso*-1 or *meso*-2 species. If both pyramidal inversion and ring reversal processes were contributing to the changes in NMR bandshapes then each species will exchange with the other three at rates which match the experimental NMR timescale. Information from two-dimensional NMR exchange experiments, (2D-EXSY), (see later) indicates only one rate process lies within the NMR detection timescale. This is attributed to pyramidal chalcogen inversion by virtue of the expected rates of such a process [1,7] and to the fact that the bridge reversal process is likely to be rapid due to the low torsional barriers associated with M–S or M–Se (M = Cr, Mo, W) bonds. In the analogous Pd^{II} and Pt^{II} complexes $[Fe(C_5H_4SR)_2MX_2]$ (X = Cl or Br), for example, the low torsional barriers of Pd–S and Pt–S bonds were considered the prime causes of the very rapid bridge reversal fluxion in these complexes [7], in contrast to complexes such as $[Fe(C_5H_4S)_2S]$ where the S–S torsional barrier is relatively high and leads to slow bridge reversal [18].

The assumption of rapid bridge reversal in the present complexes implies that there is rapid exchange between adjacent structures on the front and rear faces of the cube diagram (Fig. 1), and that the NMR spectral changes are due solely to

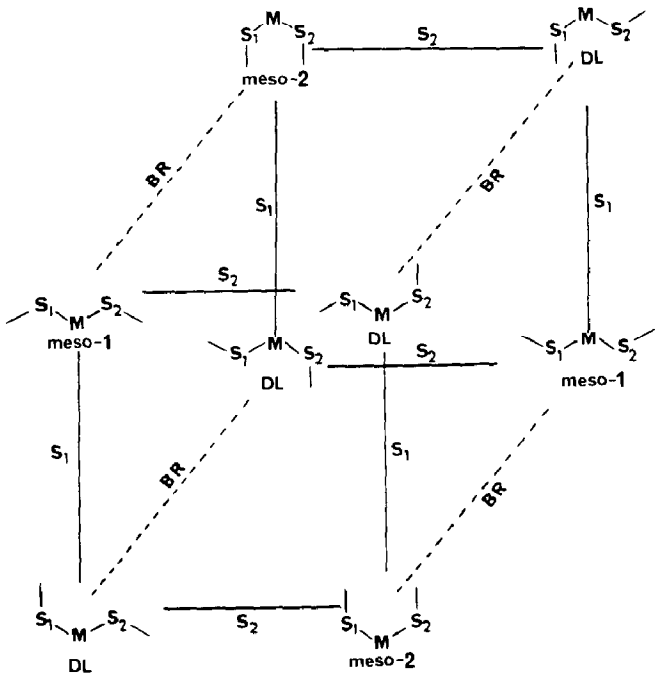

Fig. 1. Graph diagram showing the relationships of the static invertomer species of $[M(CO)_4\{(C_5H_4SCH_3)_2Fe\}]$. BR = bridge reversal, S_1, S_2 = pyramidal S inversion.

chalcogen inversion which interchanges bridge reversal-averaged DL and *meso* species. The degenerate DL pairs will thus appear as averaged pseudo-planar –E–M–E-bridge structures while the *meso*-1/*meso*-2 averaging will be strongly weighted in favour of the *meso*-1 structure by virtue of the high steric crowding of the E-methyls in *meso*-2 both with each other and with the adjacent ring protons. Chalcogen pyramidal inversion thus exchanges the species according to

$$\begin{array}{ccc} \langle meso\text{-}1/meso\text{-}2\rangle & \rightleftharpoons & \langle DL/DL\rangle \\ \approx meso\text{-}1 & & \\ \Updownarrow & & \Updownarrow \\ \langle DL/DL\rangle & \rightleftharpoons & \langle meso\text{-}2/meso\text{-}1\rangle \\ & & \approx meso\text{-}1 \end{array}$$

The two sets of signals observed in the low temperature ^1H NMR spectra are thus attributed to these two conformationally averaged species. The identification of the more populous species required further experiments. This species in the case of the complex $[W(CO)_4(BMSEF)]$ was unambiguously identified from its low temperature $^{13}C\text{-}\{^1H\}$ spectrum (Table 3). At $-40\,^\circ C$, the carbonyl region exhibited two strong signals, each with ^{183}W satellites, plus three weak signals. The former arise from the $\langle DL/DL\rangle$ invertomer (where both axial carbonyls are equivalent) and the latter are due to the *meso*-1 species (where the axial carbonyls are non-equivalent). The ring carbon region comprises four strong and four weak signals, but provides no unequivocal distinction between the DL and *meso* forms since both give rise to the same number of signals. The ^{77}Se NMR spectrum of the same complex was also recorded (Table 3). The more intense DL signal shows ^{183}W satellites ($^1J(SeW) =$

Table 3

^{13}C and ^{77}Se NMR data for complex **6** in CD_2Cl_2 at $-40\,^{\circ}C$

Complex	Invertomer	$\delta(^{13}C)$				$\delta(^{77}Se)$ [f]
		E-Me carbons	ring carbons	axial CO	equatorial CO	
δ	DL	23.38[49.5] [a]	81.02[134.5] [b], 76.19 75.54[18.0] [c] 73.15, 71.85	203.61[131.0] [d]	207.59[170.0] [d]	85.22[41.5] [g]
	meso	22.04	75.02 [e], 73.68 70.19	206.71 200.82	208.30	76.41

[a] ^1J(SeC). [b] ^1J(SeC), quaternary ring carbon. [c] ^2J(SeC). [d] ^1J(WC). [e] Two *meso* signals were undetected. [f] Relative to Me_2Se_2. [g] ^1J(WSe).

41.5 Hz) while the *meso* signal was too weak to reveal its ^{183}W satellites.

The relative populations of the invertomers vary somewhat throughout the complex series (Table 2) but the DL species is invariably dominant, being 93% abundant in the case of $[Mo(CO)_4(BMSEF)]$ at $-60\,^{\circ}C$. There appears to be a slight dependence on the steric bulk of the Group 6 metal moiety (viz. the selenium complexes **2**, **4**, and **6**), but a more pronounced dependence on the chalcogen present, (viz. complexes **5** and **6**) where the *meso* invertomer is more favoured for the BMSF complex than for the BMSEF complex.

Dynamic NMR studies

Having established that the NMR bandshape changes are due to varying rates of pyramidal chalcogen inversion the energetics of the process were investigated using

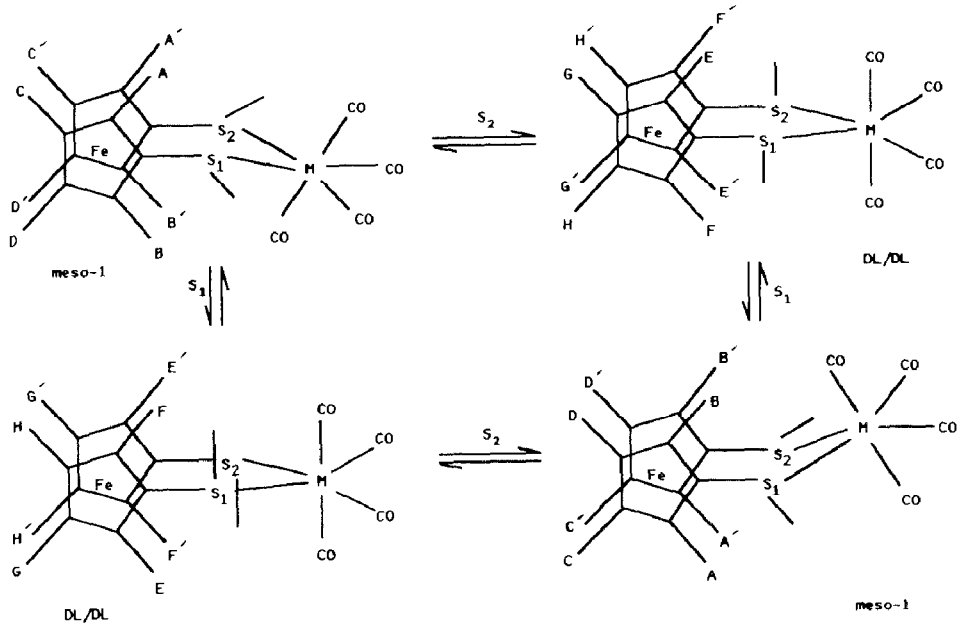

Fig. 2. The bridge-reversal-averaged invertomers of the complexes showing the methine proton labelling.

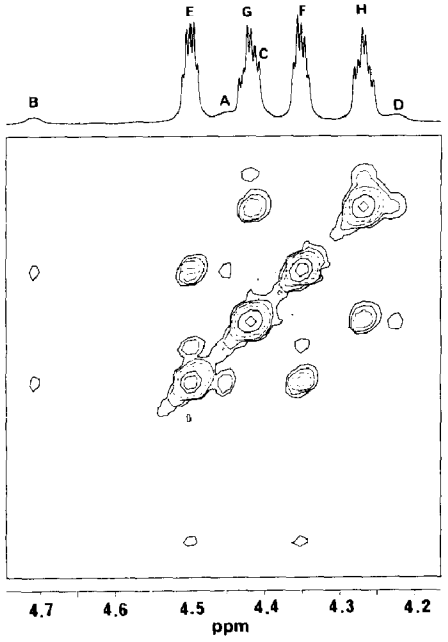

Fig. 3. The ^{1}H 2D-EXSY spectrum of [W(CO)$_4$(BMSEF)] at $-30\,^\circ$C, showing the two sets of exchanging methine signals.

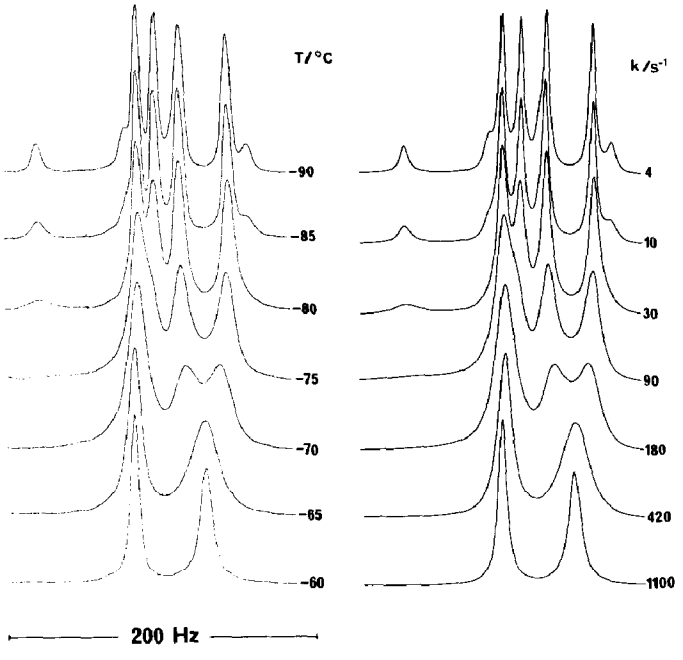

Fig. 4. The experimental and computer synthesised spectra (methine region) of [W(CO)$_4$(BMSF)] showing the 'best-fit' rate constants for each temperature.

the ring methine protons as the structural probes. (The S-methyl signals of the DL and *meso* species were insufficiently differentiated for accurate DNMR analyses). The methine protons are labelled according to Fig. 2. Each solution species constitutes an 8-spin system and the full dynamic problem is defined as

$$\begin{array}{ccc} AA'BB'CC'DD' & \rightleftharpoons & EF'FE'GH'HG' \\ \uparrow\downarrow & & \uparrow\downarrow \\ FE'EF'HG'GH' & \rightleftharpoons & BB'AA'DD'CC' \end{array}$$

Such a spin problem is too large to be handled by our standard DNMR program [11] and in order to reduce the computation to manageable proportions, all proton–proton scalar couplings were neglected. The three-bond couplings (viz. $^3J_{AC}$, $^3J_{BD}$, $^3J_{CD}$, etc.) are estimated to be of the order of 2.5 Hz and the four-bond couplings (viz. $^4J_{AB}$, $^4J_{AD}$, $^4J_{BC}$, etc.) of the order of 1.3 Hz [18]. These magnitudes are small compared to the chemical shift separations of the ring protons and their contributions to the observed bandshapes of the methine signals will be very slight at temperatures where there is substantial exchange broadening. Accordingly, the dynamic spin problem can be reduced to two sub-systems of single spins exchanging between four different chemical configurations, namely

$$\begin{array}{ccc} \textit{meso}\ A & \rightleftharpoons & E\ DL \\ \uparrow\downarrow & & \uparrow\downarrow \\ DL\ F & \rightleftharpoons & B\ \textit{meso} \end{array} \quad + \quad \begin{array}{ccc} \textit{meso}\ C & \rightleftharpoons & G\ DL \\ \uparrow\downarrow & & \uparrow\downarrow \\ DL\ H & \rightleftharpoons & D\ \textit{meso} \end{array}$$

This problem is easily handled, *providing* the two sets of four exchanging signals can be correctly identified. This proved possible from 2D-EXSY experiments at low temperature. The ^{1}H 2D-EXSY spectrum of [W(CO)$_4$(BMSEF)] (Fig. 3) illustrates how this assignment problem can be solved.

The four strong signals are due to the ⟨DL/DL⟩ species and the weak set to *meso*-1. (One signal of the latter is not resolved due to overlap with a ⟨DL/DL⟩ signal). Inspection of the cross-peaks in this 2D spectrum identifies the four exchanging signals of the A/E/B/F set and the three observable signals of the C/G/D/H set. Unambiguous distinction between pairs of DL and *meso* signals in each sub-spectrum was not possible and the labelling in Fig. 3 must be regarded as tentative. In particular, the signal labels E/F, G/H, and C/D could possibly be interchanged. The assignments of signals A and B are more certain, as the signal at considerably higher frequency to the rest arises from the near proximity of proton B to the de-shielding zone of the adjacent axial carbonyl function of the *meso*-1 species. Fortunately, the bandshape analyses are not dependent on the correct assignment of *individual* methine signals, only on the correct separation of the eight signals into the two exchanging sets. Total bandshape analyses were performed in the temperature range −60 to 15 °C and excellent fits obtained. The results for [W(CO)$_4$(BMSF)] are shown in Fig. 4, where the 'best-fit' rate constants refer to *meso*-1 → ⟨DL/DL⟩ exchanges. Rate constants for direct exchange between *meso* environments (e.g. A ⇌ B) or between ⟨DL/DL⟩ environments (e.g. E ⇌ F) were taken as zero despite the observation of cross-peaks relating these signals. Such synchronous double inversion processes are known to be negligibly slow [8] and the observed cross-peaks are second-order artifacts arising from the choice of mixing time in the EXSY pulse sequence.

Table 4

Arrhenius and Eyring activation parameters for pyramidal chalcogen inversion (*meso* → DL) in the complexes **2**, **4**, **5**, and **6**

Complex	E_a (kJ mol^{-1})	$\log_{10}(A)$ (s^{-1})	$\Delta H^{\ddagger}$ (kJ mol^{-1})	$\Delta S^{\ddagger}$ (J K^{-1} mol^{-1})	$\Delta G^{\ddagger}$ (298 K) (kJ mol^{-1})
2	115.5 ± 3.5	25.8 ± 0.7	113.3 ± 4.7	242 ± 14	41.3 ± 0.6
4	96.0 ± 2.4	22.5 ± 0.5	93.9 ± 2.4	178 ± 10	40.7 ± 0.5
5	60.6 ± 1.2	17.8 ± 0.3	59.0 ± 1.2	92.2 ± 6.0	31.5 ± 0.6
6	92.6 ± 1.3	20.3 ± 0.3	90.5 ± 1.3	136.9 ± 4.8	49.6 ± 0.2

The activation parameters associated with the *meso*-**1** → ⟨DL/DL⟩ interconversion for the complexes **2**, **4**, **5** and **6** are given in Table 4. The energy barriers, as expressed by $\Delta G^{\ddagger}$ (298 K) values, are somewhat lower than normal [1,7] but display the expected trends, namely that S inversion is of appreciably lower energy than Se inversion (cf. complexes **5** and **6**) and the inversion barriers fall in the order W > Cr > Mo (viz. complexes **6**, **2** and **4**). This ordering has been observed for other L–L complexes [1,19] and is controlled by a combination of the effects of metal electronegativity and $p\pi$–$d\pi$ stabilization of the transition state.

Particularly noteworthy features of these activation parameters are the large values of $\log_{10}A$ and $\Delta S^{\ddagger}$. Such magnitudes usually indicate intermolecular dynamic processes but no such explanation is valid here as pyramidal inversions of chalcogen atoms coordinated to transition metals invariably involve an intramolecular mechanism via a planar transition state [1]. These large values of $\Delta S^{\ddagger}$ are *not* a function of poor bandshape fittings or a neglect of systematic errors in their calculation [20]. Very high quality fittings of experimental and computer synthesised spectra were obtained over a wide temperature range for the present complexes. These unexpectedly high $\Delta S^{\ddagger}$ values were clearly a reality as they caused the NMR band coalescences to occur over a much narrower temperature range than normal. In our view the abnormally high magnitudes of the activation parameters A and $\Delta S^{\ddagger}$ may be the result of the rapid ring conformational process present in these complexes. In Fig. 2, exchanges between *meso*-**1** and ⟨DL/DL⟩ species do *not* simply involve a change in relative positioning of the S-methyl group, but require the pseudo-six-membered ring to flex from a chair form in *meso*-**1** to a pseudo-planar geometry in the averaged ⟨DL/DL⟩ species. The transition state structure is therefore likely to be highly flexible, possessing many more vibrational and rotational degrees of freedom than either ground state structure. An overall change of this type is likely to be associated with large positive A and $\Delta S^{\ddagger}$ values, and low resultant $\Delta G^{\ddagger}$ values. In the related complexes $[Fe(C_5H_4SR)_2MX_2]$ ($M = Pd^{II}, Pt^{II}$; R = alkyl) [7] no unexpected magnitudes of activation parameters were noted, and the sulphur inversion processes caused NMR exchange broadenings over a considerably wider temperature range than in the present complexes. While rapid bridge reversal was again postulated to be occurring in these complexes, the NMR bandshape changes were now due solely to exchange between pseudo-planar ⟨DL/DL⟩ pairs, since no *meso* species were detected in solution. Such exchanges do *not* involve any net conformational changes of the pseudo-six-membered ring, and thus the bridge reversal fluxion does not affect the nature of the pyramidal inversion transition state in any way.

Table 5

Fractional atomic coordinates ($\times 10^4$) for [W(CO)$_4$(BMSEF)]

Atom	x	y	z
W	2315.6(2)	1454.9(3)	1312.7(3)
Fe	815.6(7)	2966.5(13)	3697.2(11)
Se(1)	1303.1(5)	3590.3(8)	770.9(8)
Se(2)	1168.4(5)	93.5(9)	1986.4(8)
O(1)	1662(6)	491(8)	−1543(7)
O(2)	3314(4)	2819(9)	3887(7)
O(3)	3413(5)	−1156(7)	1976(7)
O(4)	3601(5)	2775(8)	239(8)
C(1)	1845(7)	791(10)	−500(9)
C(2)	2910(6)	2343(10)	2985(9)
C(3)	2986(5)	−180(10)	1704(8)
C(4)	3101(6)	2324(10)	650(9)
C(5)	288(5)	2805(11)	−296(9)
C(6)	1658(8)	−1620(11)	2873(12)
C(7)	980(5)	4077(9)	2234(8)
C(8)	1517(6)	4565(10)	3380(8)
C(9)	1054(7)	5031(10)	4167(10)
C(10)	228(7)	4837(11)	3462(11)
C(11)	177(6)	4255(10)	2255(9)
C(12)	975(6)	918(9)	3431(8)
C(13)	1560(6)	1386(9)	4552(9)
C(14)	1141(7)	1901(11)	5395(9)
C(15)	313(7)	1752(10)	4785(10)
C(16)	200(6)	1150(10)	3538(10)

X-ray crystallography

Atomic parameters for the crystal structure of [W(CO)$_4$(BMSEF)] are given in Table 5. Two views of the molecule drawn with the program ORTEP [21] and

Table 6

Bond distances (Å) [a]

Se(1)–W	2.674(4)	Se(2)–W	2.692(4)
C(1)–W	2.032(12)	C(2)–W	2.024(12)
C(3)–W	1.941(11)	C(4)–W	1.936(12)
C(7)–Fe	2.033(10)	C(12)–Fe	2.033(11)
C(8)–Fe	2.070(11)	C(13)–Fe	2.050(12)
C(9)–Fe	2.073(12)	C(14)–Fe	2.067(11)
C(10)–Fe	2.060(12)	C(15)–Fe	2.059(12)
C(11)–Fe	2.071(12)	C(16)–Fe	2.042(12)
C(5)–Se(1)	1.975(11)	C(6)–Se(2)	1.958(12)
C(7)–Se(1)	1.926(10)	C(12)–Se(2)	1.905(10)
C(1)–O(1)	1.138(12)	C(2)–O(2)	1.135(12)
C(3)–O(3)	1.187(12)	C(4)–O(4)	1.188(13)
C(7)–C(8)	1.417(13)	C(12)–C(13)	1.428(14)
C(8)–C(9)	1.430(14)	C(13)–C(14)	1.437(16)
C(9)–C(10)	1.440(17)	C(14)–C(15)	1.418(17)
C(10)–C(11)	1.426(15)	C(15)–C(16)	1.454(15)
C(11)–C(7)	1.430(13)	C(16)–C(12)	1.420(14)

[a] Esd's, given in parentheses, are applicable to the least significant digits.

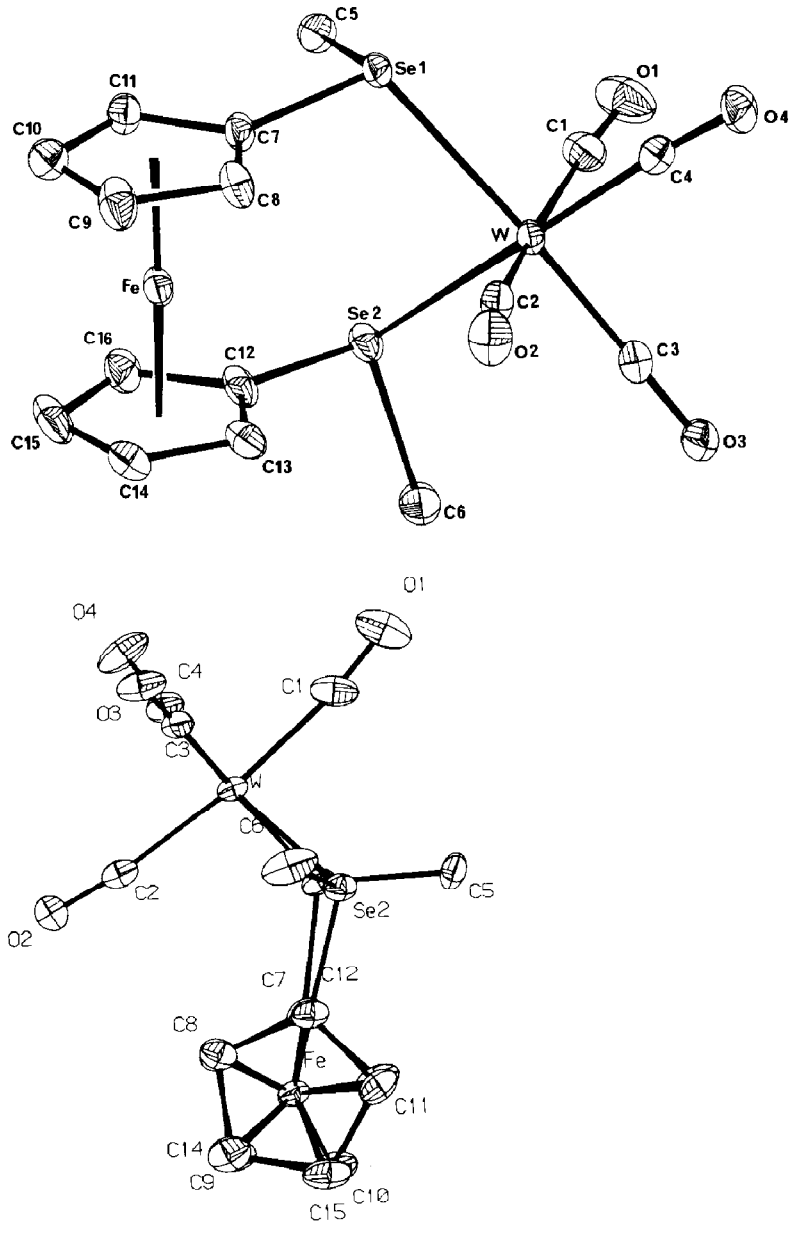

Fig. 5. Two views of the X-ray crystal structure of $[W(CO)_4(BMSEF)]$.

indicating the numbering scheme adopted are shown in Fig. 5. This displays the expected six-coordination for W, the chelating nature of the ligand and the DL conformation of the molecule. This is in accord with the solution NMR studies discussed earlier. Bond distances and bond angles are noted in Tables 6 and 7 respectively.

The range of C–C distances in the cyclopentadienyl rings, (1.417(13) to 1.454(15) Å) and the iron to carbon distances (2.033(10) to 2.073(12) Å) are within the ranges expected for ferrocenyl compounds. The two W–Se distances are similar and lie

Table 7

Selected bond angles (°) [a]

Se(1)–W–Se(2)	86.3		
C(2)–W–Se(1)	90.3(4)	C(1)–W–Se(1)	88.5(4)
C(4)–W–Se(1)	94.7(4)	C(3)–W–Se(1)	175.9(3)
C(2)–W–Se(2)	100.4(4)	C(1)–W–Se(2)	90.0(4)
C(4)–W–Se(2)	173.6(3)	C(3)–W–Se(2)	89.7(4)
C(7)–Se(1)–W	110.1(4)	C(6)–Se(2)–W	107.1(5)
C(7)–Se(1)–C(5)	98.9(5)	C(12)–Se(2)–C(6)	95.4(5)
C(8)–C(7)–Se(1)	123.3(7)	C(13)–C(12)–Se(2)	126.7(8)
C(11)–C(7)–Se(1)	125.7(8)	C(16)–C(12)–Se(2)	123.5(8)
C(11)–C(7)–C(8)	110.1(9)	C(16)–C(12)–C(13)	109.8(9)
C(9)–C(8)–C(7)	107.5(9)	C(14)–C(13)–C(12)	107.3(10)
C(10)–C(9)–C(8)	107.1(10)	C(15)–C(14)–C(13)	107.9(10)
C(11)–C(10)–C(9)	109.3(10)	C(16)–C(15)–C(14)	108.8(10)
C(10)–C(11)–C(7)	105.9(10)	C(15)–C(16)–C(12)	106.2(10)

[a] Esd's, given in parentheses, are applicable to the least significant digits.

within the range, 2.588(2) to 2.736(2) Å, of values found in the four reported structures containing W(O) bonded to Se [22–25]. The present study appears to be the only diffraction study reported in which W(O) is bonded to two Se atoms.

Inspection of the bond angles at W, Table 7, shows that there is considerable distortion from an octahedral structure at W. Differences in the ferrocenyl exocyclic C–C–Se bond angles (means 123.4 and 126.2°) are observed. These can be compared with values of 123.8 and 127.2° in bis(ferrocene 1,1′-diselenato)tin(IV) [26] and 123.8 and 127.8° in 1,3-diselena 2,2-dichlorogermyl-[3]ferrocenophane [27]. This is a structural feature which is common in ferrocenophanes of this type.

Equations for selected least-squares mean planes are given in Table 8. The cyclopentadienyl rings are planar within limits of error, and adopt an eclipsed configuration, Fig. 5. The ring planes can be considered to be parallel, the dihedral

Table 8

Equations of selected least-squares mean planes

Cyclopentadienyl ring C(7)–C(11)

$0.09474X + 0.91637Y - 0.38897Z = 2.79476$

Deviations (Å)

C(7)	−0.0075	C(10)	−0.0020	C(5)	−0.1322
C(8)	0.0075	C(11)	0.0067		
C(9)	−0.0041	Se(1)	0.2615		

Cyclopentadienyl ring C(12)–C(16)

$0.10364X + 0.91203Y - 0.39680Z = -0.56092$

Deviations (Å)

C(12)	−0.0068	C(15)	−0.0053	C(6)	−1.8660
C(13)	0.0045	C(16)	0.0083		
C(14)	0.0002	Se(2)	−0.0437		

angle between them being only 0.72°. This compares with dihedral angles of 5.6 and 6.1° respectively for the tin and germanium [3]ferrocenophanes mentioned earlier. The two Se atoms are displaced from the mean planes to which they are attached, but by widely differing amounts, namely 0.26 Å for Se(1) and 0.04 Å for Se(2). This gives rise to a non-bonded Se–Se distance of 3.67 Å. The van der Waals radius for Se was found [28] to be 1.80 to 1.85 Å. The C(7) to C(12) separation is 3.329 Å and so without a displacement of the Se atoms from the ring planes, the Se atoms would be in too close contact.

Acknowledgements

We wish to thank the University of Exeter for a Frank Southerden Scholarship (to N.J.L.), and the SERC for use of the single crystal X-ray diffraction service (Queen Mary College, London) and of the high field NMR service (University of Warwick).

References

1 E.W. Abel, S.K. Bhargava, and K.G. Orrell, Prog. Inorg. Chem., 32 (1984) 1.
2 K.G. Orrell and V. Šik, Ann. Rep. NMR Spectrosc., 19 (1987) 79.
3 D.F. Shriver, Manipulation of Air-Sensitive Compounds, McGraw-Hill, New York, 1969.
4 M.A. Bennett, L. Pratt and G. Wilkinson, J. Chem. Soc., (1961) 2037.
5 R.B. King and A. Fronzaglia, Inorg. Chem., 5 (1966) 1837.
6 D.P. Tate, J.M. Augl and W.R. Knipple, Inorg. Chem., 1 (1962) 433.
7 B. McCulloch, D.L. Ward, J.D. Woollins and C.H. Brubaker, Jr., Organometallics, 4 (1985) 1425.
8 E.W. Abel, T.P.J. Coston, K.G. Orrell, V. Šik and D. Stephenson, J. Magn. Reson., 70 (1986) 34.
9 E.W. Abel, I. Moss, K.G. Orrell, V. Šik and D. Stephenson, J. Chem. Soc., Dalton Trans., (1987), 2695.
10 D.A. Kleier and G. Binsch, J. Magn. Reson., 3 (1970) 146.
11 D.A. Kleier and G. Binsch, DNMR3 Program 165, Quantum Chemistry Program Exchange, Indiana University, 1970.
12 M.B. Hursthouse, R.A. Jones, K.M.A. Malik and G. Wilkinson, J. Am. Chem. Soc., 101 (1979) 4128.
13 A.C.T. North, D.C. Phillips and F.S. Matthews, Acta Crystallogr., Sect. A, 24 (1968) 351.
14 G.M. Sheldrick, SHELX-84 Program for Crystal Structure Solution, private communication.
15 G.M. Sheldrick, SHELX-76 Program for Crystal Structure Determination and Refinement, University of Cambridge, 1976.
16 D.T. Cromer and J.B. Mann, Acta Crystallogr., Sect. A., 24 (1968) 321.
17 D.T. Cromer and D. Liberman, J. Chem. Phys., 53 (1970) 1891.
18 E.W. Abel, M. Booth and K.G. Orrell, J. Organomet. Chem., 208 (1981) 213.
19 E.W. Abel, I. Moss, K.G. Orrell and V. Šik, J. Organomet. Chem., 326 (1987) 187.
20 J. Sandström, Dynamic NMR Spectroscopy, Academic Press, London, 1982 Chapt. 7.
21 C.K. Johnson, ORTEP II: A Fortran Thermal Ellipsoid Plotting Program Crystal Structure Illustrations, ORNL Report 3794. Oak Ridge National Laboratory, Oak Ridge, Tennessee, U.S.A. 1971.
22 A. Rettenmeier, K. Weidenhammer and M.L. Ziegler, Z. Anorg. Allg. Chem., 473 (1981) 91.
23 J. Pickardt, H. Schumann, C.F. Campana and L.F. Dahl, J. Organomet. Chem., 216 (1981) 245.
24 H. Fischer, S. Zeuner and J. Riede, Angew. Chem. Int. Ed. Engl., 23 (1984) 726.
25 H. Fischer, U. Gerbing, J. Riede and R. Benn, Angew. Chem. Int. Ed. Engl., 25 (1986) 78.
26 A.G. Osborne, R.E. Hollands, R.F. Bryan and S. Lockhart, J. Organomet. Chem., 224 (1982) 129.
27 A.G. Osborne, A.J. Blake, R.E. Hollands, R.F. Bryan and S. Lockhart, J. Organomet. Chem., 287 (1985) 39.
28 A.G. Osborne, R.E. Hollands, J.A.K. Howard and R.F. Bryan, J. Organomet. Chem., 205 (1981) 395.